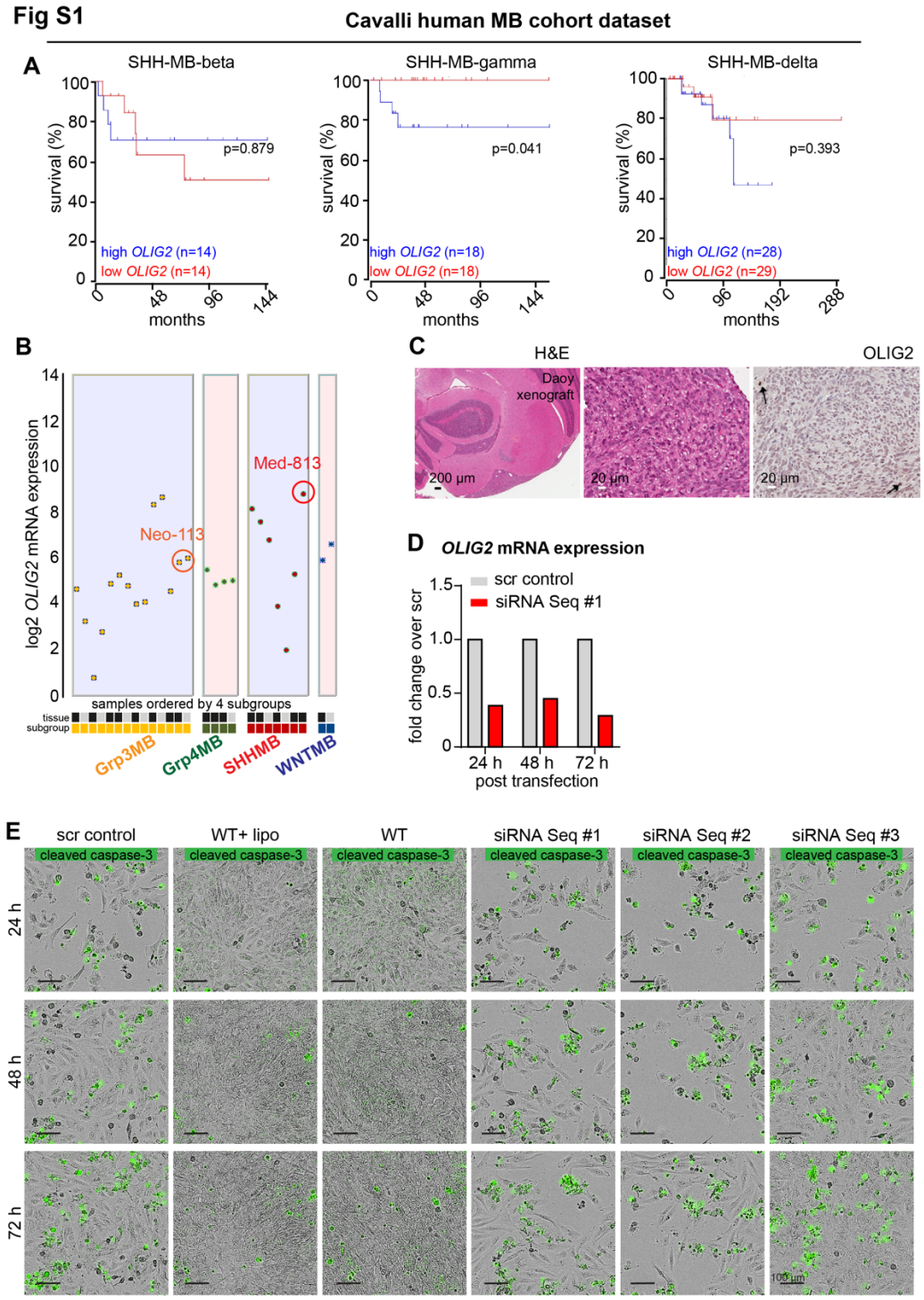

Supplementary Figure 1. OLIG2 expression in SHH-MB and OLIG2 siRNA knockdown studies.

(A) Kaplan-Meier curves in SHH-MB-beta, delta and gamma subtypes, based on *OLIG2* expression, which is analysed using R2 platform: https://hgserver1.amc.nl/cgibin/r2/main.cgi.

(B) *OLIG2* mRNA expression of Med-813 and Neo-113 filtered tissues analysed using R2: Genomics analysis and visualization platform: https://hgserver1.amc.nl/cgibin/r2/main.cgi.
(C) H&E and OLIG2 immunostaining in Daoy xenograft model Daoy. Arrowheads, $OLIG2^{+}$ cells. Scale bars as indicated.
(D *OLIG2* mRNA expression in Daoy cells, after transient siRNA KD.
(E) Bright field images of Daoy cells transfected with scrambled control sequence and siRNA OLIG2 KD Seq #1, #2 and #3 at 24, 48 and 72 hours. Cells labelled with cleaved caspase-3/7 are shown in green. Scale bar = 100μm.

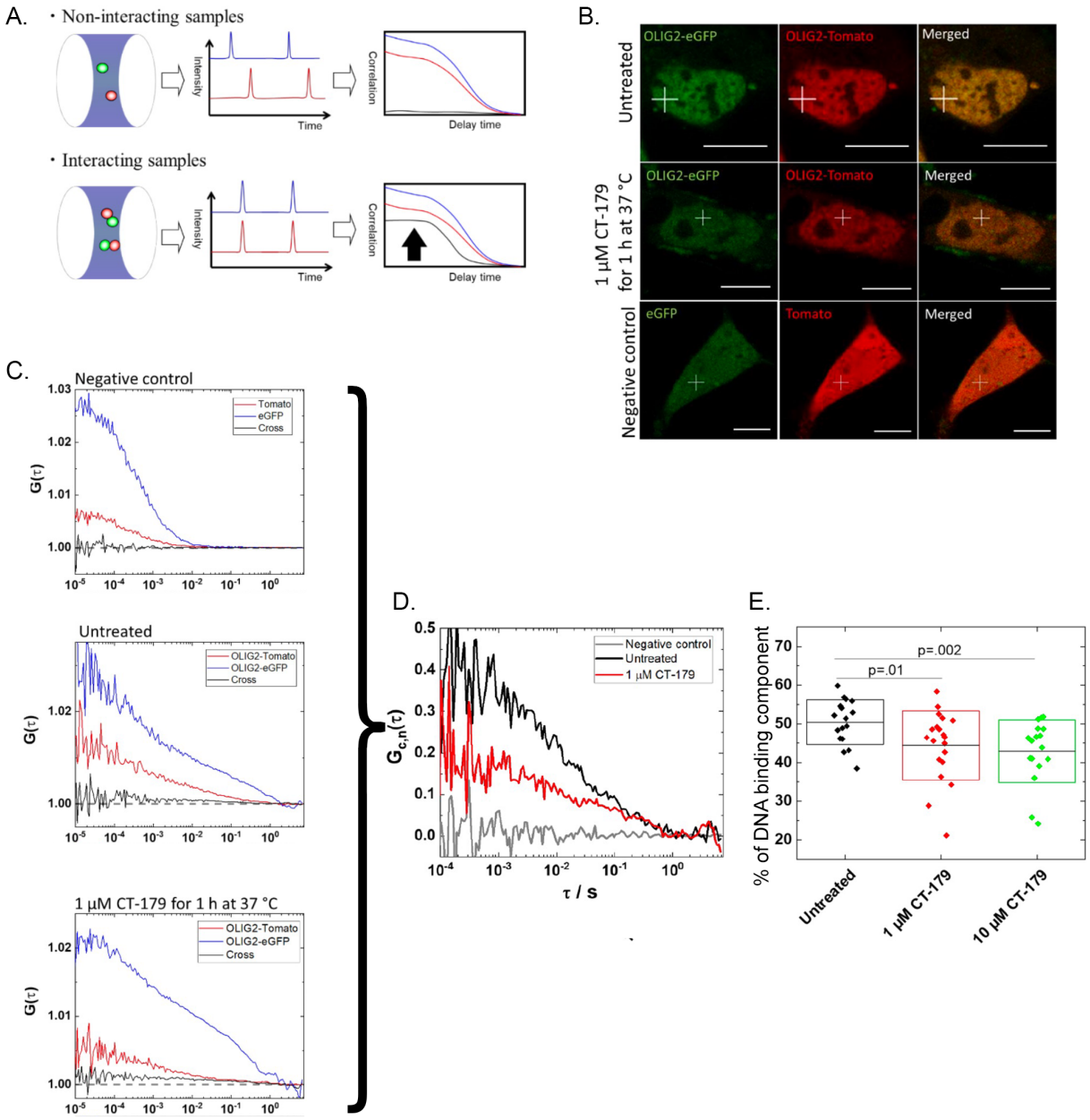

Supplementary Figure 2. FCCS analysis of CT-179 in living HEK-293 cells.

(A) Schematic showing depicting the principle of FCCS. FCCS yields three correlation curves: two autocorrelation curves (for eGFP (blue) and for Tomato (red)) and one cross-correlation curve (black). Interactions between OLIG2- eGFP and OLIG2-Tomato are reflected by the amplitude of the CCC (the less the interaction, the lower is the amplitude

of the CCC). And, conversely, the more interactions between them, the higher the amplitude.
(B) Representative images of living HEK-293 cells. The top and middle rows show nuclei of HEK-293 cells co-transfected with OLIG2-eGFP and OLIG2-Tomato fusion constructs and treated as indicated. The bottom row shows negative control cell co-transfected with eGFP and Tomato which do not localize to the nucleus in the absence of OLIG2 sequence.
(C) Representative autocorrelation curves for eGFP and Tomato and cross correlation curves for each of the conditions shown in (B).
(D) RCA for each of the indicated conditions. Highest RCA was observed in untreated HEK-293 cells co-transfected with OLIG2-eGFP and OLIG2-Tomato. Lowest RCA was observed for negative control cell co-transfected with eGFP and Tomato without OLIG2 sequence. HEK-293 cells co-transfected with OLIG2-eGFP and OLIG2-Tomato and treated with CT-179 showed RCA that was intermediate.
(E) Calculated % DNA binding in HEK-293 cells co-transfected with OLIG2-eGFP and OLIG2-Tomatoand treated as indicated.

Fig S3

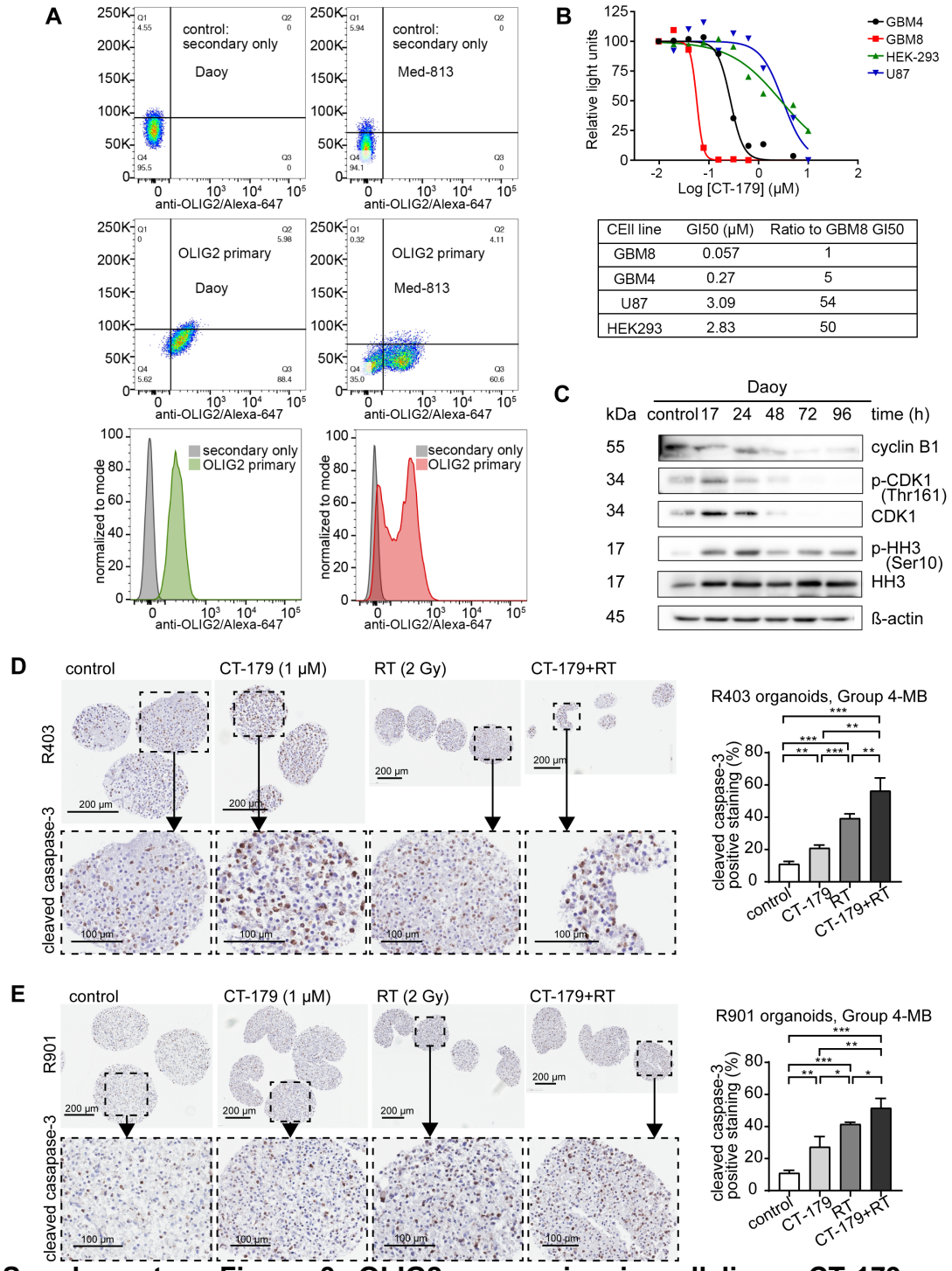

CEll line	GI50 (μM)	Ratio to GBM8 GI50
GBM8	0.057	1
GBM4	0.27	5
U87	3.09	54
HEK293	2.83	50

Supplementary Figure 3. OLIG2 expression in cell lines, CT-179 sensitivity in OLIG2-negative cell lines, effects of CT-179 on mitotic protein expression in Daoy cells, and effects of MB organoids R403 and R901

(A) Flow cytometry using OLIG2 antibodies compared to secondary-only controls, shows uniform OLIG2 expression in Daoy cells and heterogeneous OLIG2 expression in Med-813 cells.

(B) Comparison of sensitivities of OLIG2-expressing cell lines GBM8 and GBM4 versus OLIG2-negative cell lines U87MG and HEK-293.
(C) Western blot showing effect of CT-179 treatment on the expression of indicated mitosis-regulating proteins in Daoy cells.
(D,E) MB organoids (D) R403 and (E) R901were treated for CT-179 or RT alone or in combination for 48 hours. IHC shows CC3, and graphs show % of cells that were CC3+ (means ± SD, n=3, *$p < 0.05$, **$p < 0.01$, ***$p < 0.001$).

Fig S4

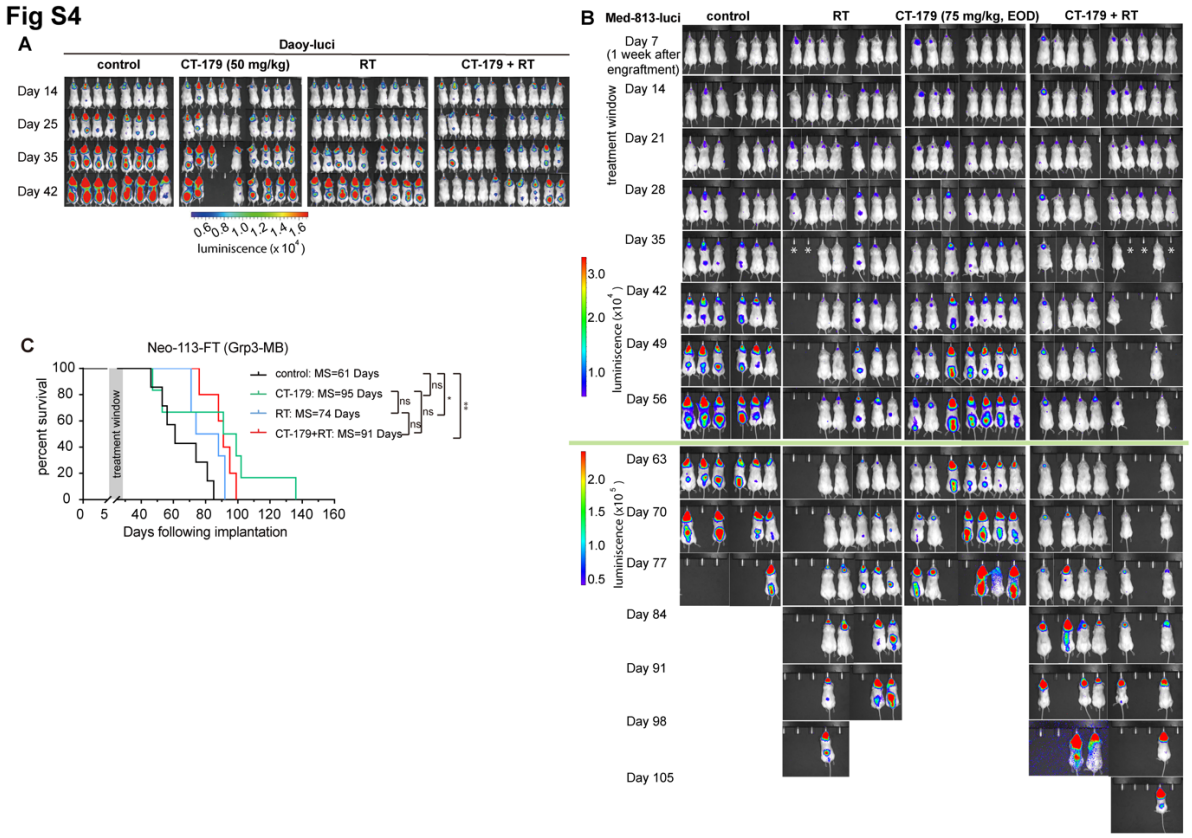

Supplementary Figure 4. Bioluminescence imaging of xenografted tumors with CT-179 treatment and EFS of Neo-113-FT

(A,B) Representative *in vivo* bioluminescence imaging of NOD *rag* gamma mice engrafted with (A) Daoy-luci cells or (B) Med-813 cells, and treated as indicated.

(C) Kaplan-Meier survival curves of Neo-113-FT (≥ 4 per group) treated with indicated therapies (*p < 0.05, **p < 0.01, ***p < 0.001). MS: median survival.

Fig S5

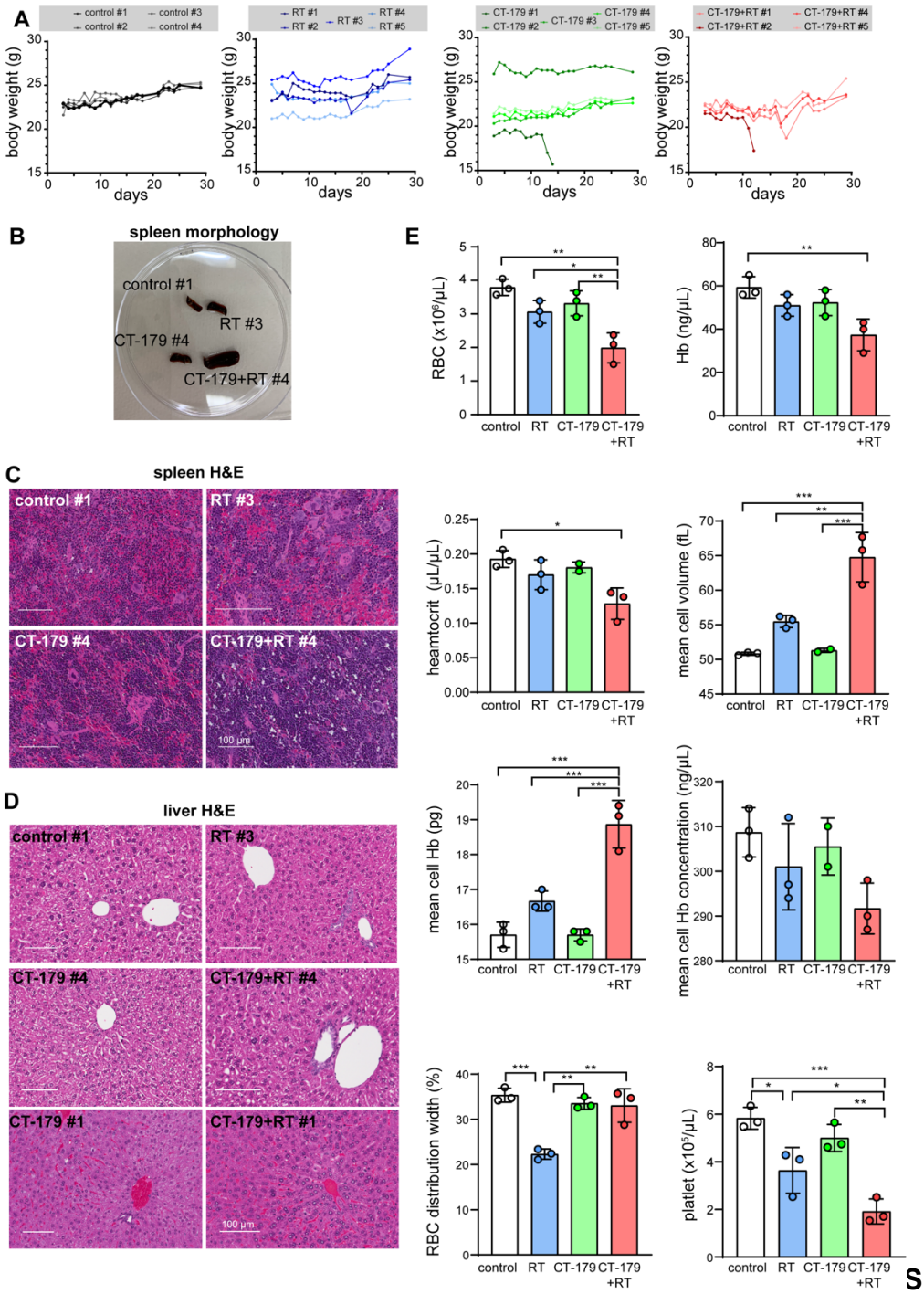

Supplementary Figure 5. Toxicity studies of CT-179 treatment in NRG mice, including healthy controls and tumor models.

(A) Body weight of healthy NRG mice mice throughout the treatment and post treatment. Mice were assigned into 4 treatment groups, including vehicle (n=4), CT-179 (n=5), RT

(n=5) and combination (n=4). Mice were euthanised on day 30 post commencement of treatment.
(B) Spleens on day 30 post-commencement of treatment (one spleen from each treatment group). The spleen from mouse treated with CT-179 in combination with RT was significant enlarged.
(C) The histopathology of the spleen. Light microscope histological tissue slides of spleen from mice euthanised on day 30 post-commencement of treatment. Control spleen section showing normal splenic architecture. Mouse treated with RT (RT#3) has ill-defined spleen section with diffused white pulp. Distorted lymphoid architecture and giant macrophages, presence of giant macrophages can be seen from CT-179 treated spleen. Presence of granular leukocytes in between lymphocytes in lymphoid follicles besides giant macrophages can be observed in mouse treated with combination treatment.
(D) Histopathology of the mouse liver post treatment. Control, RT, CT179#4 and CT-179+RT#4 liver sections showing normal hepatic architecture, whereas livers from CT-179#1 and CT-179+RT#1 presented with haemorrhage features. The mice CT-179#1 and CT-179+RT#1 died in the middle of the treatment.
(E) Full blood counts (excluding white blood cells) from mice euthanised on day 30 post-commencement of treatment. Bar graphs representing the red blood cell (RBC), haemoglobin (Hgb), haematocrit (Hct), mean cell volume (MCV), mean cell haemoglobin (MCH), mean cell haemoglobin concentration (MCHC), red blood cell distribution width (RDW) and platelet (Plt). RBC and Plt were significant lower when compared to the other treatment groups. Graphs display data from each individual animal from three independent experiments with each n=3. Statistical significance was determined using Student's t test (means ± SD, n=3, *$p < 0.05$, **$p < 0.01$, ***$p < 0.001$).

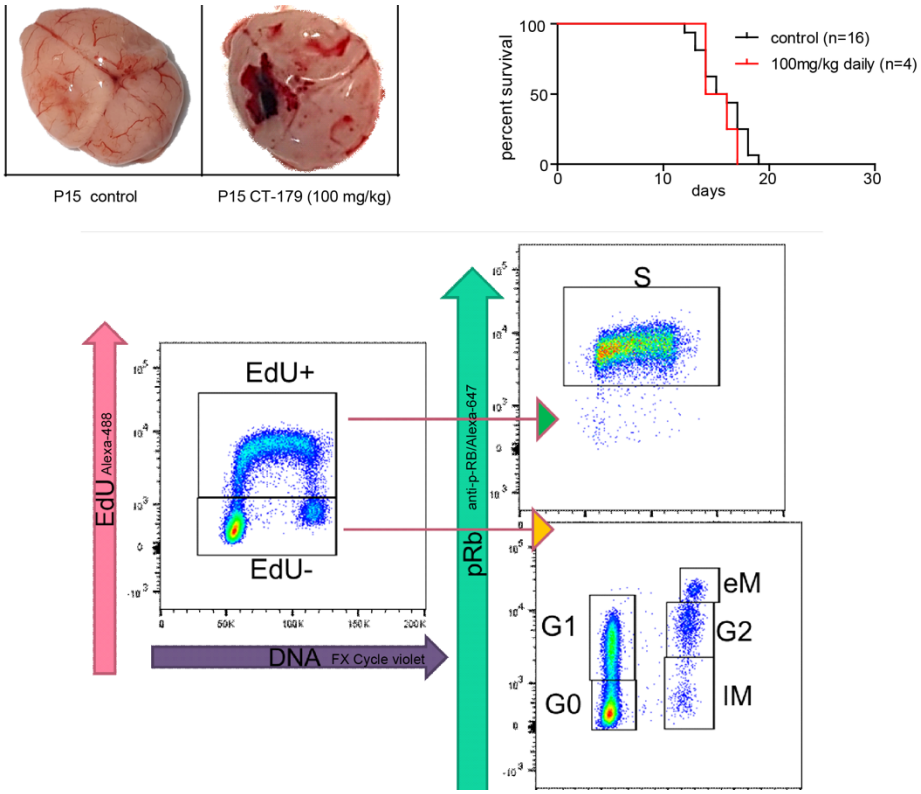

Supplementary Figure 6. Brain toxicity with dosing above MTD in *G-Smo* model and gating strategy used for flow cytometry measurement of cell cycle dynamics in *G-Smo* MBs.

(A) Representative brains showing typical examples for hemorrhage after 100 mg/kg CT-179 treatment in *G-Smo* mice.
(B) Kaplan-Meier survival curve of *G-Smo* mice treated with control and CT-179 daily (100 mg/kg).
(C) Flow cytometry cell cycle gating strategy was used to quantify dissociated tumour cells at G_0, G_1, S, and G_2/M phases.

Fig S7

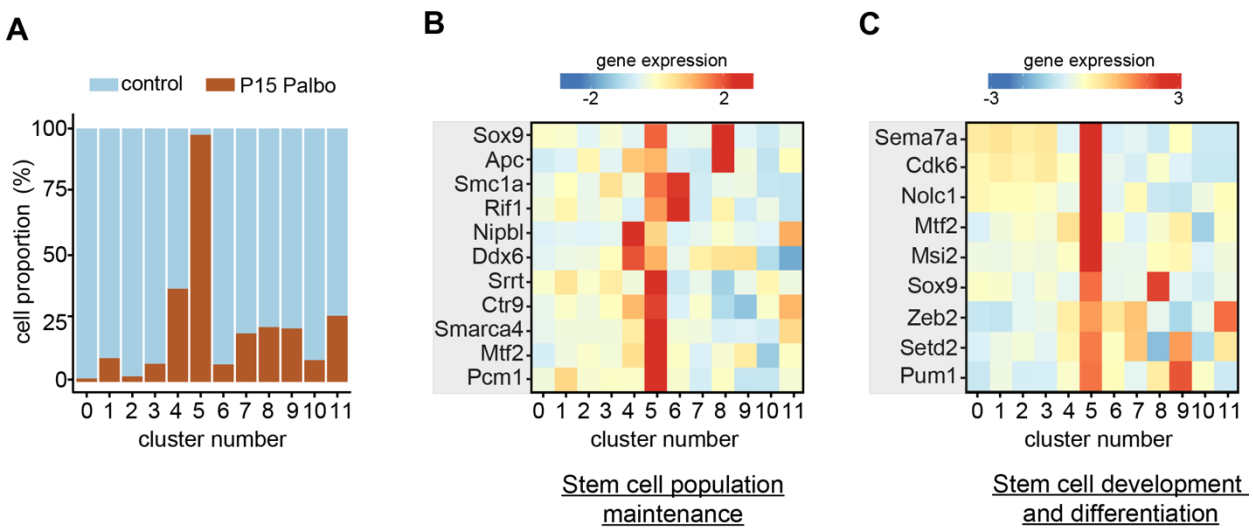

Supplementary Figure 7. Single-cell transcriptomic analysis defines a role of stem cell-associated genes in POx-Palbociclib drives resistance.

(A) Bar plot of cell proportions from control and POx-Palbociclib-treated tumors in each of the 12 tumor cell clusters. Cells of Cluster 5 were specifically induced by POx-Palbociclib treatment.
(B,C) Heat maps showing differential gene expression of (C) stem cell maintenance–associated genes, and (D) stem cell development and differentiation-associated genes. Stem cell-related genes were consistently enriched in Cluster 5.